AUTEX Research Journal, Vol. 20, No 4, December 2020, DOI 10.2478/aut-2019-0026

THE EFFECT OF ELECTRIC FIELD ON NANOFIBERS PREPARATION IN CYLINDRICAL-ELECTRODE-ASSISTED SOLUTION BLOWING SPINNING

Wenxing Zheng[1,2], Wenyu Zheng[3], Xinhou Wang[1]*

1 College of Textiles, Donghua University, Shanghai 201620, China
2 College of Light Industry and Textile, Qiqihar University, Qiqihar 161000, China
3 College of Civil Engineering and Architecture, Nanyang Normal University, Nanyang 473061, China
E-mail: xhwanglarry@163.com

Abstract:

Cylindrical-electrode-assisted solution blowing spinning (CSBS) is a novel nanofiber preparation method. The electric field of CSBS not only is one of the main innovations of this technology but also plays a key role in the preparation of nanofibers. In this article, the electric field of CSBS and the influences of electric field on the preparation of nanofibers were studied systematically for the first time by simulations, theoretical analyses, and experiments. This paper innovatively established the coaxial capacitor model for studying the CSBS electric field. The effects of electric field on the preparation and morphology of CSBS nanofibers were theoretically investigated by using this model. The theoretical formulas that can express the relationships between the various electric field variables were obtained. The electric field strength distribution, voltage distribution, and the relationships between the electric field parameters of CSBS were obtained by finite element simulations. The simulations' results show that reducing the diameter of cylinder (DC) or increasing the voltage increase the electric field strength of the jet surface. Experimental results reveal that increasing voltage or reducing DC can reduce the diameter of nanofibers. The experimental and simulation results prove the correctness of the theoretical research conclusions. The theoretical and simulation conclusions of this paper lay a theoretical foundation for further study of CSBS electric field. The experimental conclusions can directly guide the controllable preparation of CSBS nanofibers.

Keywords:

Nanofibers; Cylindrical-electrode-assisted solution blowing spinning; Morphology; Electric field; Simulation.

1. Introduction

As a traditional nanofiber preparation method, solution blowing spinning (SBS) [1] has received special attention in the past decade due to its high productivity [1-3] and versatility. Like many functional fibers [4], nanofibers fabricated by SBS have been widely used in filtration [5, 6], energy [7-10], and biomedical applications [11-13]. However, the SBS nanofibers have some inevitable defects, including larger diameter, bad continuity, and more slag balls [14, 15]. These defects hinder the applications of SBS. A novel nanofiber preparation technique named cylindrical-electrode-assisted solution blowing spinning (CSBS) has been reported in our previous article [16]. The structures of nanofiber nonwoven prepared by CSBS are similar to the SBS ones. However, compared with SBS fibers, the standard deviation of diameter of CSBS nanofibers drops by 21% and the average diameter of CSBS nanofibers decreases by 6.17%. Since CSBS nanofibers are finer and more uniform than SBS nanofibers, this may make CSBS nanofiber webs more suitable for filtration and other applications than SBS ones [16].

The CSBS has a different spinning mechanism than other conventional nanofiber preparation techniques such as electrospinning, SBS, and centrifugal spinning. First, CSBS produces excellent quality nanofibers by air shearing force plus electrostatic force. In addition, the jet of the CSBS system is charged due to the electrostatic induction effect. Therefore, the principles of traditional nanofiber preparation technologies cannot explain and study CSBS well. This also led to the study of the CSBS electric field still in a blank state. However, the electric field of CSBS plays a key role in the preparation of nanofibers. Moreover, the addition of the cylindrical-assisted-electrode is one of the most important innovations of CSBS. Therefore, it is very necessary to conduct an in-depth and comprehensive study of the electric field of CSBS.

This paper aims to study the electric field of CSBS and the effect of electric field on the preparation of CSBS nanofibers by theoretical, simulation, and experimental methods. According to the characteristics of the CSBS, this paper established the "coaxial cylindrical capacitor model" using the principle of electrostatic induction and other related electrical knowledge and innovatively used this model to investigate the electric field of the CSBS system. The theoretical formulas that can express the relationships between the various electric field variables were obtained. This paper also used these formulas to explain the effect of electric field on the preparation and morphology of CSBS nanofibers. In this work, the finite element simulation software Ansoft Maxwell was used to simulate the CSBS

electric field. The electric field strength distribution, voltage distribution, and the relationships between the electric field parameters were obtained by simulations. The effects of electric field parameters (voltage and diameter of cylinder (DC)) on the morphology of nanofibers were studied by two groups of experiments. This paper also discussed the consistency of experimental, simulation, and theoretical research conclusions.

2. Method and apparatus

As the Figure 1 depicts, the CSBS setup consists of an air compressor (A), a custom-made die (B), a microsyringe pump (C), a syringe (D), a blunt needle (E), a hollow metal cylinder (F), a high-voltage source (G), and an earthed metal receiver (H).

The spinning solution was pumped to the blunt needle (E) by a hypodermic syringe (D). The high-pressure air was delivered to the custom-made die (B) by the oil-less compressor (A). The power supply (G) was connected to the cylindrical electrode (F) through a wire, and the cylindrical electrode (F) was charged by the power supply (G). When spinning solution stream was forced out of the needle tip (E), it was subsequently stretched by the high-velocity airflow, which was blown from the home-made die (B), and traveled to the collector (H). When the flying jet approached the cylinder (F), it was non-contact charged by the electric field around the charged cylinder (F) due to the electrostatic induction effect [16]. The nanofibers were finally formed on the receiver (H). During the charged jet flying toward the receiver (H), the diameter of the jet reduced because of the solvent evaporation. The thinning of the jet caused an increase in the surface charge density of the jet. When the surface charge density of the jet increased to a certain extent, the jet splitted due to the mutual repulsion of the same charges [16, 17]. This splitting may occur repeatedly during the spinning process. Each split would split the jet into several finer jets, thus achieving the effect of reducing the fiber diameter [16]. That is to say, the jet in the CSBS system is stretched and attenuated by the combination of the air-stretch and electrostatic forces. The solution jet of CSBS is charged by a non-contact electrostatic induction effect. So the mechanism of CSBS is different from other traditional nanofiber preparation methods (such as electrospinning, SBS, and centrifugal spinning). Different flow rates, air pressures, and electric field intensities around the cylindrical electrode could be obtained by adjusting the feed rate of the microsyringe pump (C), the air pressure of the air compressor (A), and the voltage of the power supply (G), respectively.

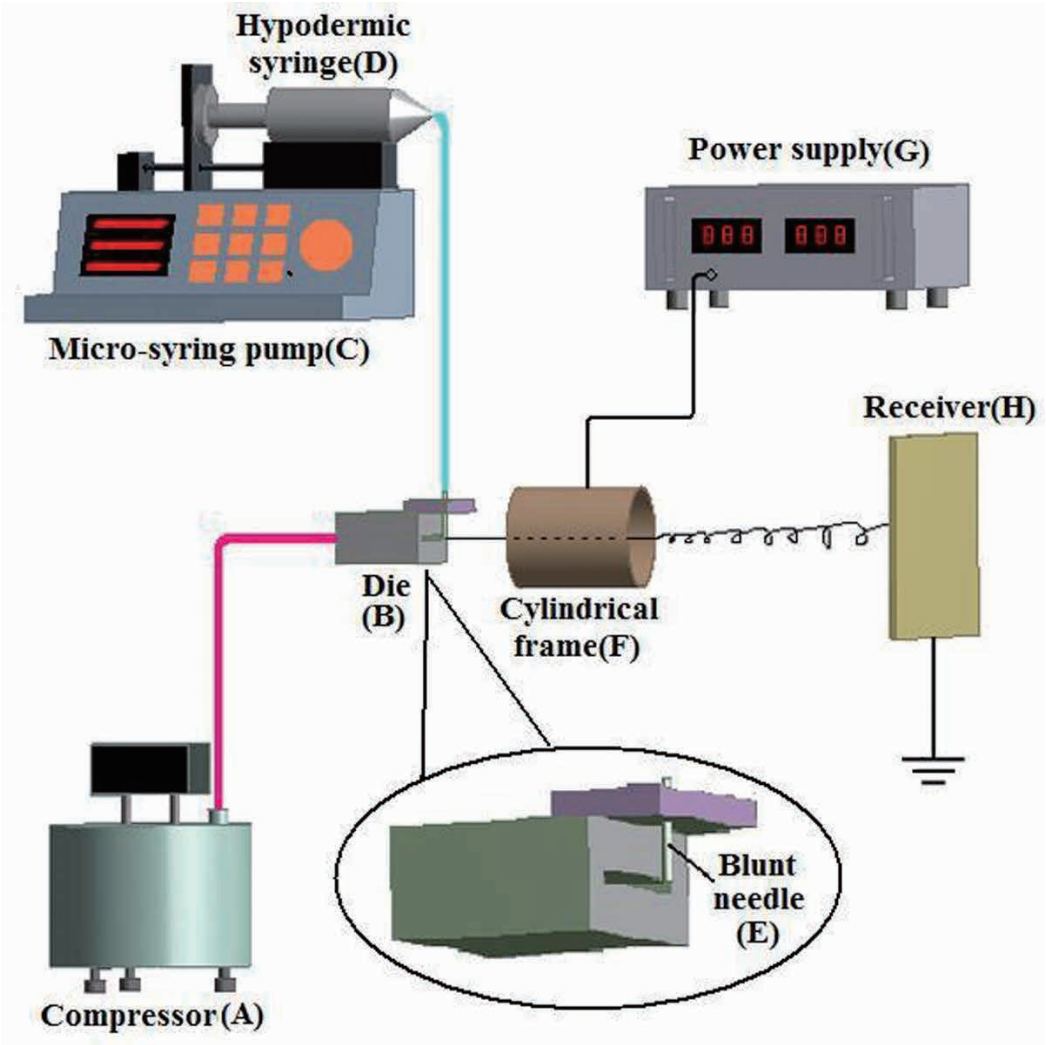

Figure 1. Schematic of CSBS system [16]

3. Theoretical and simulation analyses

3.1 Theoretical analysis

In the spinning process of the conventional electrospinning technology, the power source is directly connected to the solution jet. The power supply directly charges the solution jet. However, the CSBS technique charges the jet by non-contact electrostatic induction. That is to say, CSBS and electrospinning have different mechanisms for charging the jet. The theories of electrospinning cannot thoroughly describe and explain the electric field of CSBS. Therefore, it is necessary to conduct a theoretical study on the electric field of CSBS. One of the main innovations of CSBS compared to traditional SBS is the addition of the cylindrical electrode. Thus, this paper mainly studied the electric field between the cylindrical electrode and the jet.

In the CSBS process, when the jet is close to the cylindrical electrode, the jet is charged due to the electrostatic induction effect. According to the principle of electrostatic induction, the quantity of charges carried by the jet and the cylindrical electrode is the same. Assume that the quantities of surface charge on both the jet and the cylindrical electrode were Q. It is known from reference [15] that the effective stretching distance of high velocity air is very short from the blunt needle (≈100 μm). Within this effective distance, the shear force of the high-pressure gas stream rapidly reduces the diameter of the jet. Beyond this effective distance, the effect of the airflow stretching force on the jet diameter becomes very small. In the CSBS system, the distance from the needle to the cylindrical electrode is much larger than 100 μm. Therefore, the stretching of the air has little effect on the diameter of the jet during the passage of the jet through the electrode. Thus, it is assumed that during the passage of the solution jet through the cylindrical electrode, the diameter of the jet did not change and the jet always traveled straight along the axis of the cylindrical electrode. A jet having the same length as the cylindrical electrode was chosen for investigation. At this time, the cylindrical electrode and the jet can be regarded as two plates of a coaxial cylindrical capacitor. This component consisting of the jet and the cylindrical electrode can be regarded as a coaxial cylindrical capacitor. The following is a study of the electric field of this coaxial cylindrical capacitor. The nonuniformity of the electric field near the edges of the plate was neglected for the convenience of discussion. The coaxial cylindrical capacitor is shown in Figure 2.

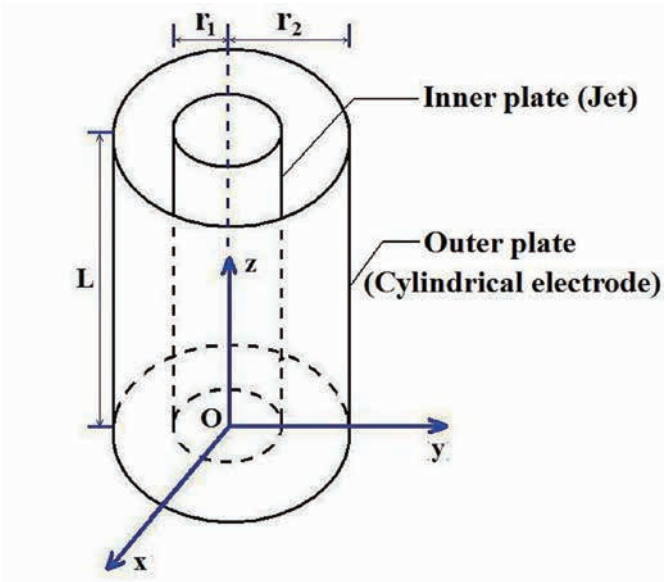

Figure 2. The schematic of the coaxial cylindrical capacitor

The cylindrical coordinate system was established based on Figure 2. Any point $P(x, y, z)$ in the rectangular coordinate system can be represented by the corresponding cylindrical coordinate $P(\rho, \theta, z)$, where $r_1 \leqslant \rho \leqslant r_2$. It can be seen that the potential V is a function of ρ and is independent of θ and z. Since there is no charge between the two cylindrical plates, the Laplace equation $\nabla^2 V = 0$ can be used to calculate the potential. Specific steps are as follows:

$$\frac{1}{\rho}\frac{\partial}{\partial\rho}\left(\rho\frac{\partial V}{\partial\rho}\right)+\frac{1}{\rho^2}\frac{\partial^2 V}{\partial\theta^2}+\frac{\partial^2 V}{\partial Z^2}=0 \quad (1)$$

where V is the electric potential.

According to the actual situation of this case, Eq. (1) can be written in the following form:

$$\frac{1}{\rho}\frac{\partial}{\partial\rho}\left(\rho\frac{\partial V}{\partial\rho}\right)=0 \quad (2)$$

Solving for V, $V = A\ln\rho + B$ (3)

where A and B are constants, and Eq. (3) can be solved by the following boundary conditions:

$V = 0$ (zero potential) at $\rho = r_1$ and

$V = U_0$ (voltage between two cylindrical plates) at $\rho = r_2$

The above boundary conditions were substituted into Eq. (3) for the values of A and B.

$$A = \frac{U_0}{\ln\frac{r_2}{r_1}} \quad B = -\frac{U_0}{\ln\frac{r_2}{r_1}}\ln r_1$$

Substituting the values of A and B into Eq. (3),

$$V = \frac{U_0}{\ln\frac{r_2}{r_1}}\ln\rho - \frac{U_0}{\ln\frac{r_2}{r_1}}\ln r_1 \quad (4)$$

where U_0 is the voltage between the two plates, r_1 is the outer diameter of the inner plate of the capacitor, and r_2 is the inner diameter of the outer plate of the capacitor.

From the potential gradient formula,

$$\vec{E} = -gradV = -\nabla V = -\left(\frac{\partial V}{\partial \rho}\vec{e_\rho} + \frac{1}{\rho}\frac{\partial V}{\partial \theta}\vec{e_\theta} + \frac{\partial V}{\partial Z}\vec{e_Z}\right)$$

Substituting Eq. (4) into the above equation,

$$\vec{E} = -\frac{U_0}{\ln\frac{r_2}{r_1}} \cdot \frac{1}{\rho}\vec{e_\rho}$$

$$E = \left|\vec{E}\right| = \left|-\frac{U_0}{\ln\frac{r_2}{r_1}} \cdot \frac{1}{\rho}\right| = \frac{U_0}{\ln\frac{r_2}{r_1}} \cdot \frac{1}{\rho} \quad (5)$$

where E is the electric field strength between the plates of the capacitor.

The surface elements ΔS were taken at the corresponding positions of the two plates, and the capacitor composed of them can be regarded as a parallel plate capacitor. The electric field between the two plates is a uniform electric field. Therefore,

$$E = \frac{\sigma}{\varepsilon_0} \quad (6)$$

where σ is the surface charge density of the plate and ε_0 is the permittivity of free space.

From Eqs. (5) and (6),

$$\sigma = \frac{\varepsilon_0 U_0}{\ln\frac{r_2}{r_1}} \cdot \frac{1}{\rho} \quad (7)$$

Let $\rho = r_1$ to find the quantity of surface charge on the jet (inner plate) (Q_{jet}):

$$Q_{jet} = \iint_S \sigma dS = \int_0^L \int_0^{2\pi r_1} \frac{\varepsilon_0 U_0}{r_1 \ln\frac{r_2}{r_1}} dl dz = \frac{2\pi\varepsilon_0 L U_0}{\ln\frac{r_2}{r_1}} \quad (8)$$

where Q_{jet} is the quantity of surface charge on the jet (inner plate) and L is the length of the cylindrical capacitor.

The surface area of jet (inner plate) is

$$S_{jet} = 2\pi r_1 L \quad (9)$$

Now we can find the surface charge density of jet:

$$\sigma_{jet} = \frac{Q_{jet}}{S_{jet}} = \frac{\varepsilon_0 U_0}{r_1 \ln\frac{r_2}{r_1}} \quad (10)$$

where σ_{jet} is the surface charge density of jet.

Substituting $\rho = r_1$ into Eq. (5) to find the surface electric field strength of jet E_{jet}:

$$E_{jet} = \frac{U_0}{r_1 \ln\frac{r_2}{r_1}} \quad (11)$$

where E_{jet} is the surface electric field strength of jet.

It can be seen from Eqs. (10) and (11) that an increase in voltage (U_0) results in an increase in surface electric field strength of jet (E_{jet}) and surface charge density of jet (σ_{jet}). According to the CSBS mechanism [16], when the charge density of jet reaches a certain amount, the jet will split into many finer jets due to mutual charge repulsion. An increase in the surface charge density of the jet causes an increase in the probability of jet splitting, which ultimately leads to finer fibers. Therefore, it can be concluded that increasing the voltage (U_0) can reduce the diameter of the CSBS nanofibers. Similarly, the decrease in the radius (r_2) of the outer plate (cylindrical electrode) can cause an increase in surface electric field strength of jet (E_{jet}) and surface charge density of jet (σ_{jet}). Thus, reducing the diameter of the cylindrical electrode (DC) can reduce the diameter of the CSBS nanofibers. As can be seen from Eq. (5), as ρ increases, electric field strength (E) decreases. In other words, the farther away from the inner plate (jet), the smaller the electric field strength.

3.2 Simulation analysis

3.2.1 Parameters and modeling

In order to verify the correctness of the theoretical research conclusions of this paper and obtain the distribution of CSBS electric field, the electric field between the cylindrical electrode and the solution jet was simulated. The 3D electric fields were investigated by the software Ansoft Maxwell (ANSYS Inc., USA) utilizing the finite element method. All the electric field intensities and voltages were calculated by the Ansoft Maxwell software. The effects of applied voltage and diameter of the cylindrical electrode (DC) on electric field intensity were investigated by two groups of simulation. The details of parameters utilized for the simulations are illustrated in Tables 1 and 2.

In this paper, the charged cylindrical electrode and a jet with the same length as the electrode were selected as the research objects. The electric field between the electrode and the jet was

Table 1. Parameters for simulation of different voltages

Parameter	Values
Voltage (kV)	4, 6, 8, 10, 12
Length of cylinder (LC) (cm)	10
Inner diameter of cylinder (DC) (cm)	15

Table 2. Parameters for simulation of different DCs

Parameter	Values
Voltage (kV)	8
Length of cylinder (LC) (cm)	10
Inner diameter of cylinder (DC) (cm)	5, 10, 15, 20, 25

studied by simulation. For ease of discussion and modeling, the following assumptions were made: when the jet passed through the electrode, the jet always flied along the axis of the electrode, while the diameter of the jet remained constant and equal to the inner diameter of the blunt needle of 0.42 mm.

The material parameters of the cylindrical electrode used for modeling were as follows: materials' name was aluminum and relative permeability and bulk conductivity were 1.000021 and 38000000 Siemens/m, respectively. Other physical geometries and process parameters were established according to their practical values in Section 4 of this paper. The model for the finite element analysis is illustrated in Figure 3. Simulations of electric field were formed after solving process and meshing of the program.

3.2.2 Electric field distribution maps

Figure 4 shows the voltage distribution simulated by the Ansoft Maxwell 3D software when the DC, LC, and applied voltage are 10 cm, 10 cm, and 8 kV, respectively. As can be seen from Figure 4, a number of coaxial equipotential surfaces are formed between the cylindrical electrode and the solution jet. The voltages on these equipotential surfaces successively decrease from the electrode to the jet. This is due to the fact that the positive high voltage was loaded on the cylindrical electrode. In this paper, ten different finite element simulations were performed according to the parameters listed in Tables 1 and 2. The voltage distributions obtained by all simulations have the same regularity, that is, the voltage from the electrode to the jet gradually decreases.

Figure 5 indicates the electric field intensity distribution when the DC, LC, and applied voltage are 15 cm, 10 cm, and 10 kV, respectively. Since the diameter of the cylindrical electrode is much larger than that of the jet, the main focus of this paper is the electric field strength around the solution jet. Figure 5 shows a partially enlarged top view of the electric field strength around the jet. The white circle at the center of Figure 5 is the solution jet, and it can be seen that many concentric rings are formed around the jet. The electric field intensity gradually decreases outward from the surface of the jet. That is to say, the farther from the solution jet, the smaller the electric field strength. This conclusion is consistent with the conclusion obtained by Eq.(5). It can be seen from Eq.(5) that an increase in ρ causes a decrease in electric field intensity. The electric field intensity distribution regularities of all ten simulations are the same, that is, the electric field intensity is gradually reduced from the jet to the electrode.

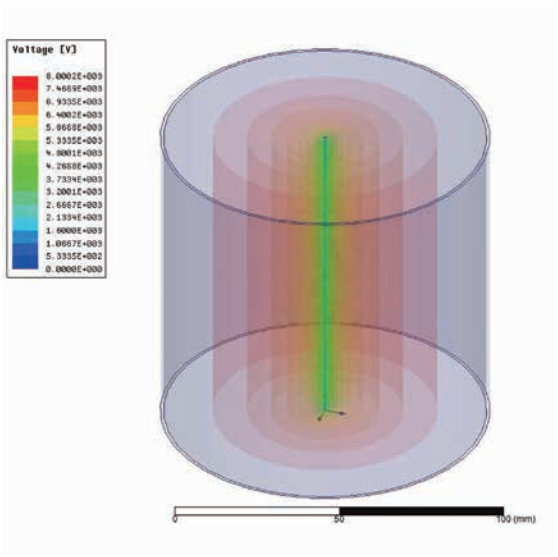

Figure 4. Simulated voltage distribution. The DC, LC, and applied voltage are 10 cm, 10 cm, and 8 kV, respectively

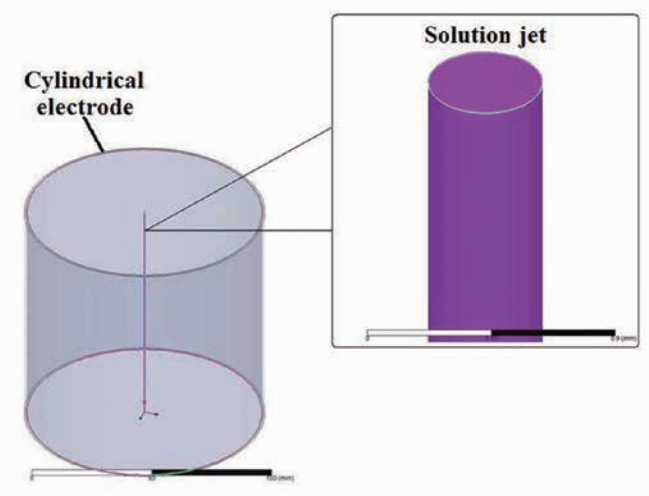

Figure 3. 3D model for simulation. The DC, LC, and diameter of the jet are 10 cm, 10 cm, and 0.42 mm, respectively

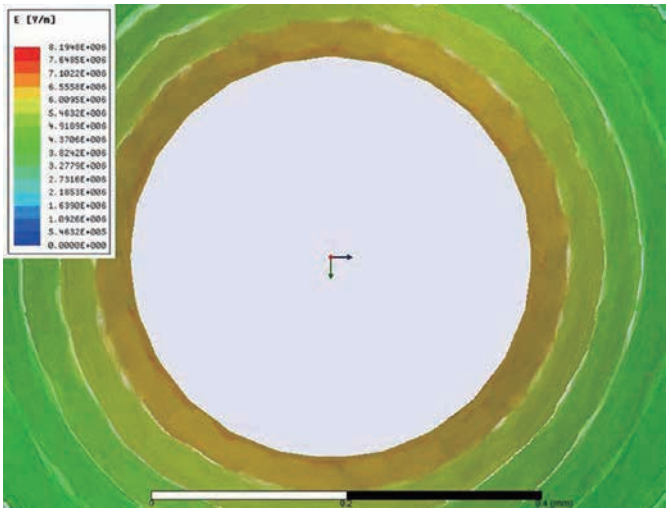

Figure 5. Simulated electric field intensity distribution. The DC, LC, and applied voltage are 15 cm, 10 cm, and 10 kV, respectively

3.2.3 Data analysis of simulation results

The data of the five finite element simulations corresponding to Table 1 were extracted. These data were plotted as Figure 6. The relationships between applied voltage, electric field strength, and distance from the jet are shown in Figure 6. It is clear that the electric field strength decreases as the applied voltage decreases, and an increase in the distance from the jet causes a decrease in the electric field strength. These conclusions are the same as those of Eq. (5). It can be seen from Eq. (5) that the electric field strength is proportional to voltage (U_0) and inversely proportional to the distance from the jet (ρ).

Similarly, the data of five simulations corresponding to Table 2 were extracted for drawing Figure 7. Figure 7 shows the relationships between DC, electric field strength and distance from the solution jet. As shown in Figure 7, the increase in DC causes a decrease in electric field strength and the electric field strength decreases as the distance from the jet increases. These conclusions can also be derived from Eq. (5). Eq. (5) shows that the electric field intensity is inversely proportional to the distance from the jet (ρ) and the natural logarithm of DC.

Because this paper mainly focuses on the electric field on the jet surface, therefore, we extracted the data of the jet surface's electric field strength and used these data to draw Figures 8 and 9. Figure 8 shows the relationship between applied voltage and the electric field intensity of the jet surface. It is clear that the electric field strength of the jet surface increases linearly with increasing applied voltage. This conclusion is the same as that of Eq. (11). Eq. (11) indicates that the electric field strength of the jet surface (E_{jet}) is proportional to the applied voltage (U_0).Figure 9 indicates the dependence of the electric field intensity of the jet surface on the DC. The conclusion of Figure 9 is consistent with the conclusion of Eq. (11). Eq. (11) shows that the electric field strength of the jet surface (E_{jet}) is inversely proportional to the natural logarithm of DC, while Figure 9 indicates that as the DC increases, the electric field intensity of the jet surface begins to decrease sharply and then the tendency to decrease gradually becomes slower.

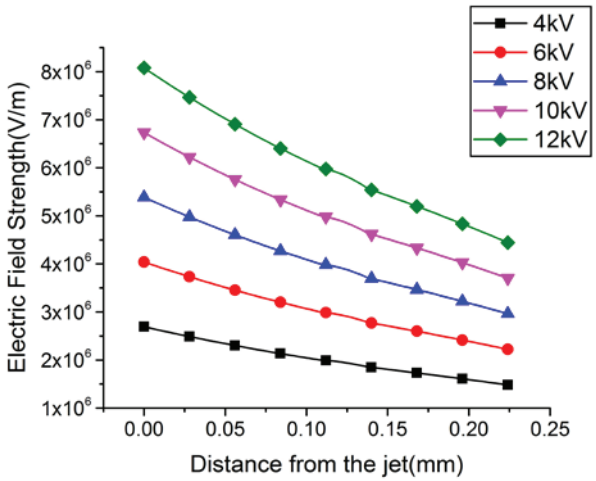

Figure 6. Effect of distance from the jet and applied voltage on electric field strength

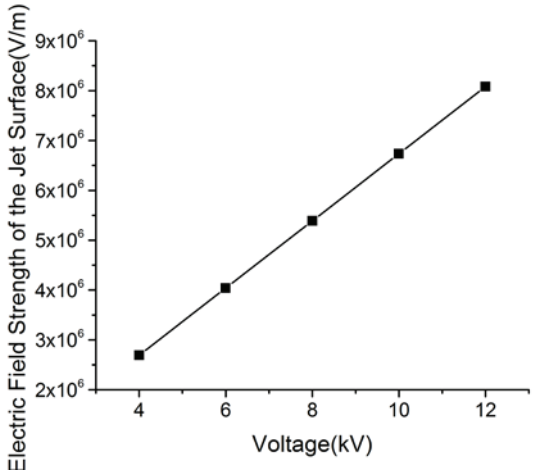

Figure 8. The relationship between applied voltage and the electric field strength of the jet surface

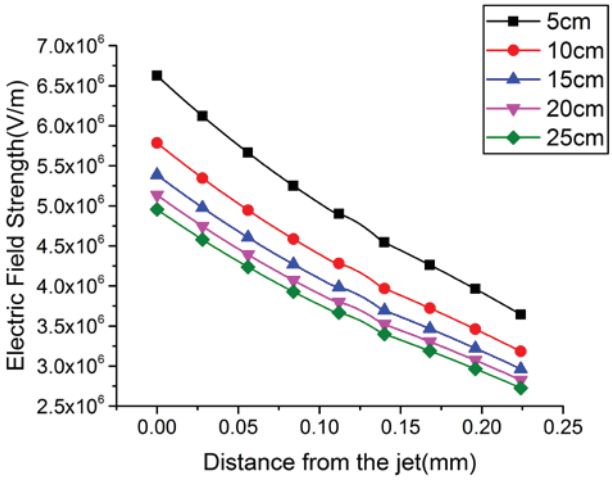

Figure 7. Effect of DC and distance from the jet on electric field strength

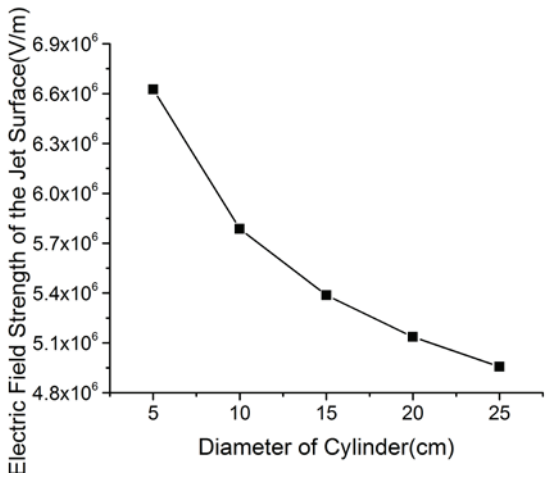

Figure 9. The relationship between DC and the electric field strength of the jet surface

4. Experimental verification and discussion

4.1 Experimental details

In this section, the effects of DC and voltage on CSBS nanofiber morphology were studied by two groups of experiments, and the experimental results were used to verify the correctness of the conclusions obtained by the theoretical analyses. The detail spinning conditions for each experiment are illustrated in Tables 3 and 4.

The polyethylene oxide (PEO) solution (viscosity ≈23,000 mPa×S) with concentration of 7% was obtained by dissolving PEO powder (weight-average molecular weight = 10^6; Shanghai Liansheng Chemical Co., Ltd., China) in distilled water. Nanofiber nonwoven samples were prepared using the CSBS equipment according to the experimental process parameters listed in Tables 3 and 4. The length, inner diameter, and outer diameter of the blunt needle were 38, 0.42, and 0.72mm, respectively. The morphology of each sample was observed by using a scanning electron microscope (SEM) (S-3400; Hitachi, Japan) after gold coating. Finally, the CSBS nanofiber diameters were measured from the SEM images by using Image J software (National Institutes of Health, USA). For each sample, four SEM photos were taken and at least 80 random measurements were taken to calculate the average diameter of CSBS nanofibers.

Table 3. Spinning conditions of different DCs

Parameter	Values
Voltage (kV)	8
Length of cylinder (LC) (cm)	10
Diameter of cylinder (DC) (cm)	5, 10, 15, 20, 25
Needle to cylinder distance (NCD) (cm)	5
Left face of cylinder to collector distance (CCD) (cm)	95
Feed rate (ml/h)	0.2
Air pressure (MPa)	0.01

Table 4. Spinning conditions of different voltages

Parameter	Values
Voltage (kV)	4, 6, 8, 10, 12
Length of cylinder (LC) (cm)	10
Diameter of cylinder (DC) (cm)	15
Needle to cylinder distance(NCD) (cm)	5
Left face of cylinder to collector distance (CCD) (cm)	95
Feed rate (ml/h)	0.2
Air pressure (MPa)	0.01

4.2 Effect of the DC on the nanofiber diameter

SEM images of PEO nanofibers prepared at DC of 5, 10, 15, 20, and 25 cm as shown in Figure 10 (a)–(e), respectively. The relationship between DC and the nanofiber diameter is shown in Figure 11. Figure 11 demonstrates that increasing the DC from 5 to 25 cm increases the average nanofiber diameter from 621.643 to 721.1224 nm. In other words, a decrease in DC resulted in a decrease in the diameter of CSBS nanofibers. In Section 3.1, it was also concluded that reducing the DC could reduce the CSBS nanofiber diameter. These data validate the correctness of the theoretical research conclusion. The explanation for this experiment result is as follows: as the DC decreases, the charge density per unit area on the cylindrical electrode increases, resulting in an increase in the electric field strength of the cylindrical electrode cavity. The increase in electric field strength makes the effect of electrostatic induction more pronounce. As a result, the surface charge density of the spinning jet increases, and finally, the fiber diameter decreases due to the increase in the splitting frequency of the jet.

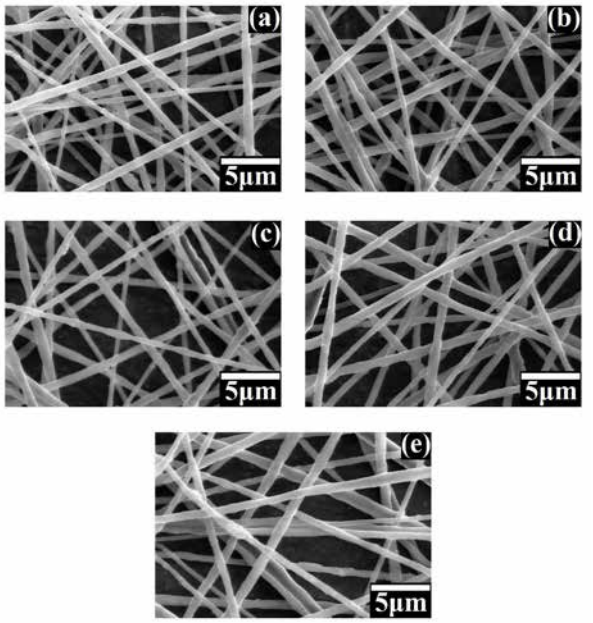

Figure 10. SEM images of PEO nanofiber mats fabricated by the CSBS system at the DC: (a) 5 cm, (b) 10 cm, (c) 15 cm, (d) 20 cm, and (e) 25 cm

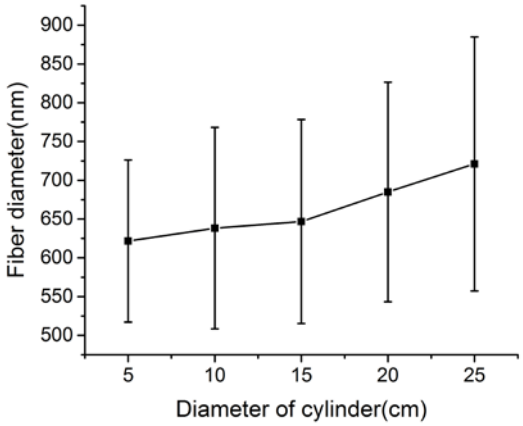

Figure 11. Relationship between DC and the fiber diameter

4.3 Effect of voltage on the nanofiber diameters

Scanning electron microscopy images of CSBS fiber formations obtained at voltages of 4, 6, 8, 10, and 12 kV are shown in Figure 12 (a)–(e), respectively. The dependence of the fiber diameter on voltage is shown in Figure 13. When the voltage is increased from 4 to 12 kV, the average diameter of fibers decreases from 670.282 to 587.882 nm as shown in Figure 13. That is, the diameter of CSBS nanofibers decreases as the applied voltage increases. This conclusion is the same as the conclusion given in Section 3.1 of this article, which verifies the correctness of the theoretical analysis in practice. The above experimental result can be explained as follows: as the voltage increases, the electric field intensity inside the cavity in the cylindrical electrode increases. The increase in electric field strength makes the electrostatic induction effect more apparent. As the jet passes through the cylinder, the amount of charge on the surface of the jet increases due to the electrostatic induction effect. As a result, the charge density of the jet increases. The increased charge density of the jet results in an increased frequency of charged jet splitting and, finally, decreases the nanofiber diameter.

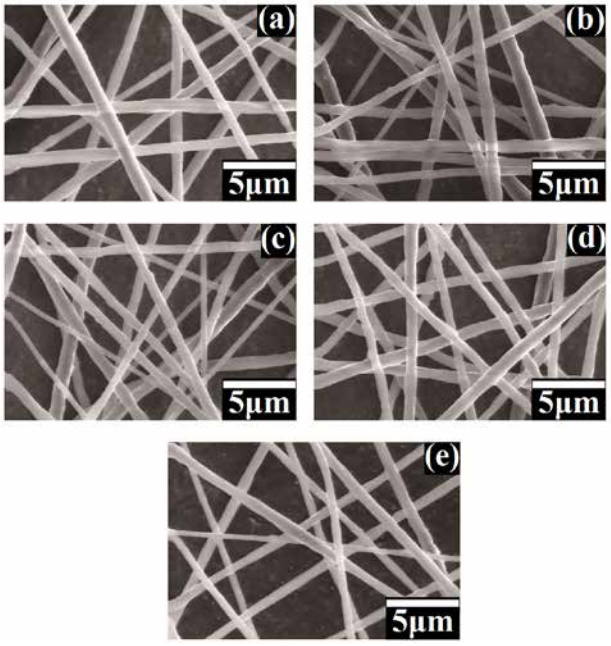

Figure 12. SEM photos of nanofibers obtained at voltages (a) 4 kV, (b) 6 kV, (c) 8 kV, (d) 10 kV, and (e) 12kV

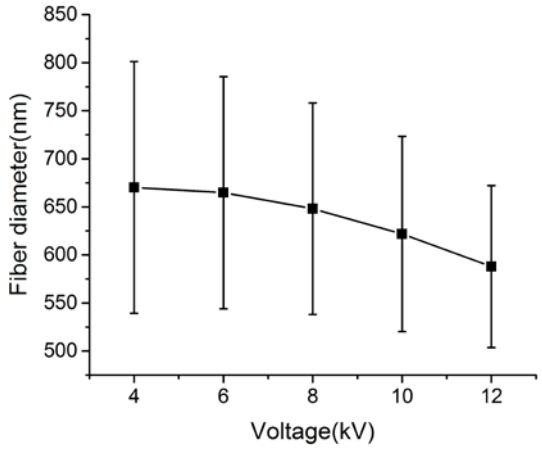

Figure 13. The relationship between the fiber diameter and voltage

5. Conclusions

In this work, the electric field of CSBS was studied systematically by using theoretical analyses, simulations, and experiments. The effects of the electric field on the preparation of nanofibers were researched in depth. The coaxial cylindrical capacitor model was established by the principle of electrostatic induction and other related electrical knowledge, and this model was innovatively used to investigate the electric field of the CSBS. In this paper, the influences of electric field parameters on the preparation and morphology of nanofibers are theoretically explained. The theoretical study concluded that increasing the voltage or decreasing the DC causes the charge density of the jet surface to increase, which ultimately leads to a decrease in the diameter of the nanofiber. The theoretical formulas of the electric field between the cylindrical electrode and the jet in the CSBS spinning system were derived. These theoretical formulas revealed the relationships between the various electric field variables of CSBS. Two groups of experiments concluded that increasing the voltage or reducing the DC reduces the diameter of the nanofibers. This conclusion is the same as the conclusion of the theoretical study, which proves the correctness of theoretical research. In this article, the finite element simulation software Ansoft Maxwell was used to simulate the electric field of the CSBS. The electric field strength distribution, voltage distribution, and the relationships between the electric field parameters of CSBS electric field were obtained by simulations. The results of the simulation are consistent with the conclusions of the theoretical study. The theoretical research and simulation conclusions in this paper can be used for further research on CSBS theories, and the experimental conclusions of this work can guide the preparation of high-quality CSBS nanofibers. The research conclusions in this paper not only fill the blank of CSBS electric field research but also are very beneficial to the application and research of CSBS technology in the fields of membrane, battery, and filtration.

Acknowledgements

Support from the National Natural Science Foundation of China (no. 51776034) is highly appreciated.

References

[1] Medeiros, E. S., Glenn, G. M., Klamczynski, A. P., Orts, W. J., Mattoso, L. H. C. (2009). Solution blow spinning: A new method to produce micro- and nanofibers from polymer solutions. Journal of Applied Polymer Science, 113(4), 2322-2330.

[2] Tutak, W., Sarkar, S., Lin-Gibson, S, Farooque, T. M., Jyotsnendu, G., et al. (2013). The support of bone marrow stromal cell differentiation by airbrushed nanofiber scaffolds. Biomaterials. 34(10), 2389-2398.

[3] Polat, Y., Pampal, E. S., Stojanovska, E., Simsek, R., Hassanin, A., et al., (2016). Solution blowing of thermoplastic polyurethane nanofibers: A facile method to produce flexible porous materials. Journal of Applied Polymer Science, 133(9), n/a-n/a.

[4] Zhang, X., Shi, M. (2018). Flame retardant vinylon/poly(m-phenylene isophthalamide) blended fibers with synergistic flame retardancy for advanced fireproof textiles. Journal of Hazardous Materials, 365, 9-15.

[5] Hsiao, H.-Y., Huang, C.-M., Hsu M.-Y., Chen, H. (2011). Preparation of high-surface-area PAN-based activated carbon by solution-blowing process for CO2 adsorption. Separation and Purification Technology, 82, 19-27.

[6] Tao, X., Zhou, G., Zhuang, X, Cheng, B., Li, X., et al. (2015). Solution blowing of activated carbon nanofibers for phenol adsorption. RSC Advances,. 5(8), 5801-5808.

[7] Shi, S., Zhuang, X., Chengab, B., Wang, X. (2013). Solution blowing of ZnO nanoflake-encapsulated carbon nanofibers as electrodes for supercapacitors. Journal of Materials Chemistry A, 1(44), 13779.

[8] Zhuang, X., Jia, K., Cheng, B., Feng, X., Shi, S., et al. (2014). Solution blowing of continuous carbon nanofiber yarn and its electrochemical performance for supercapacitors. Chemical Engineering Journal, 237, 308-311.

[9] Xu, X., Li, L., Wang, H., Li, X., Zhuang, X. (2015). Solution blown sulfonated poly(ether ether ketone) nanofiber–Nafion composite membranes for proton exchange membrane fuel cells. RSC Advances, 5(7), 4934-4940.

[10] Wang, H., Zhuang, X., Li, X., Wang, W., Wang, Y., et al. (2015). Solution blown sulfonated poly(ether sulfone)/poly(ether sulfone) nanofiber-Nafion composite membranes for proton exchange membrane fuel cells. Journal of Applied Polymer Science, 132(38), n/a-n/a.

[11] Behrens, A. M., Casey, B. J., Sikorski, M. J., Wu, K. L., Tutak, W., et al. (2014). In situ deposition of PLGA nanofibers via solution blow spinning. ACS Macro Letters, 3(3), 249-254.

[12] Abdal-hay, A., Sheikh, F. A., Lim, J. K. (2013). Air jet spinning of hydroxyapatite/poly(lactic acid) hybrid nanocomposite membrane mats for bone tissue engineering. Colloids and Surfaces B: Biointerfaces, 102, 635-643.

[13] Bilbao-Sainz, C., Chiou, B.-S., Valenzuela-Medina, D., Du, W. X., Gregorski, K. S., et al. (2014). Solution blow spun poly(lactic acid)/hydroxypropyl methylcellulose nanofibers with antimicrobial properties. European Polymer Journal, 54, 1-10.

[14] Li, L., Kang, W., Zhuang, X., Shi, J., Zhao, Y., et al. (2015). A comparative study of alumina fibers prepared by electro-blown spinning (EBS) and solution blowing spinning (SBS). Materials Letters, 160, 533-536.

[15] Bolbasov, E. N., Stankevich, K. S., Sudarev, E. A., Bouznik, V. M., Kudryavtseva, V. L., et al. (2016). The investigation of the production method influence on the structure and properties of the ferroelectric nonwoven materials based on vinylidene fluoride – tetrafluoroethylene copolymer. Materials Chemistry and Physics, 182, 338-346.

[16] Zheng, W., Zheng, W., Shi, C., Wang, H. (2019). Cylindrical-electrode-assisted solution blowing for nanofiber spinning. Journal of Applied Polymer Science, 136(8), 47087.

[17] Doshi, J., Reneker, D. H. (1995). Electrospinning process and applications of electrospun fibers. Journal of Electrostatics, 35(2), 151-160.